Synthesis, Characterization and Photocatalytic Activity of Au/SiO$_2$@TiO$_2$ Core-Shell Microspheres

Chengli Yao [a] and *Jinmiao Zhu* [*,a]

aSchool of Chemistry and Chemical Engineering, Hefei Normal University, 230601 Hefei, Anhui, China

By using HAuCl$_4$ as the gold precursor, spherical Au@SiO$_2$/TiO$_2$ core-shell nanostructures were prepared with the sol-gel method and ethanol reflux. The preparation process was convenient and fast. The obtained samples were characterized by UV-Vis, X-ray diffraction (XRD), field emission scanning electron microscopy (FESEM), transmission electron microscopy (TEM), X-ray diffraction (XRD) and X-ray photoelectron spectroscopy (XPS), respectively. The results suggested that these spherical particles were in uniform distribution of particle size and with excellent monodispersity. Gold nanoparticles were successfully loaded on the core-shell structure, and TiO$_2$ nanoparticles were functionalized. With the functionalization of gold nanoparticles, Au@SiO$_2$/TiO$_2$ nanoparticles showed excellent photocatalysis activity for the degradation of methyl orange. The possible mechanism of catalytic degradation was discussed in the paper.

Keywords: photocatalytic, Au@SiO$_2$/TiO$_2$, electron-hole pair, Au nanoparticles

Introduction

Because of low cost, convenient use and good environmental compatibility,[1,2] TiO$_2$ has been widely used in photocatalytic reaction, photovoltaic solar cells, hydrogen production, water separation and others.[3-6] Among these applications, most strikingly, TiO$_2$ has been used as an excellent photocatalyst for the degradation of hazardous organic pollutants.[7-9] However, the inefficient utilization of visible light or sunlight and low quantum efficiency of photocatalytic reactions, which respectively result from its relatively wide band gap (3.0-3.2 eV) requiring ultraviolet irradiation to activate it,[10,11] and the high rate of electron-hole pairs recombination, limit its applications to the great extent.[12,13] Except of large optical band gap, TiO$_2$ particles with small size are separated and recovered very difficult from the treated solution.[14] Therefore, the effective separation of electron-hole pairs and prolonging the lifetime of the holes are very advantageous for the photocatalytic degradation reaction.[15]

As a result of the great difference between the intrinsic Fermi level of the core and the conduction band energy of the (n-type) semiconductor shell, mobile electrons diffused into the core will be captured for a long time.[16] Such a metal-semiconductor material has potential applications both in electron storage and photocatalysis. Recently, it has been suggested that the presence of metal nanoparticles (NPs) might effectively capture photogenerated electrons and shift the Fermi level of TiO$_2$, which potentially prolongs the lifetime of radicals and may effectively improve the photocatalytic reduction efficiency.[17-20] Plenty of researches indicated a semiconducting shell around noble metal nanoparticles such as TiO$_2$, CeO$_2$, ZrO$_2$, could lead to a variety of optical properties and an enhancement of the catalytic activity.[21-23] Interfacial electron transfer enhanced the photocatalytic activity of a catalyst which creates and efficiently separates electron-hole pairs.[24,25] Doping of TiO$_2$ with Au NPs and Au NPs-deposited SiO$_2$-TiO$_2$ had been extensively reported.[26] The probability of photocatalytic reactions will be significantly decreased because of the fast charge recombination between the injected electrons in semiconductor NPs and the holes in Au NPs.[26] Based on literatures,[27-29] because of providing different reaction sites, tuning the optical properties of the cores, and increasing the stability of nanoparticle dispersion, the coating of silica shell on composite had been widely evaluated. These recent studies gave us insight into the composite structure of silica-coated nanoparticles. In order to further understand the role of Au nanoparticles in photocatalytic reaction and the effect of SiO$_2$ coating on such nanoparticles, Au@SiO$_2$/TiO$_2$ was fabricated by layer-by-layer coating.

*e-mail: jmzhu_chem2019@163.com

This unique structure can facilitate the photo induced charge separation and help to understand how electron transfers between semiconductors and metals. Photo degradation of methyl orange (MO) was conducted to determine the photocatalytic activity. The as-prepared material has potential applications in photo induced electron storage of solar cell and photocatalysis.

Experimental

Materials and characterization methods

In this work, tetrachloroauric acid tetrahydrate (HAuCl$_4$·4H$_2$O), sodium citrate dehydrate, titanium *n*-butoxide (TBOT), tetraethyl orthosilicate (TEOS), tetrahydrofuran (THF), ammonia (30 wt.%), isopropanol and absolute ethanol were of analytical grade and purchased from Shanghai Chemical Reagent Co. Ltd. (Shanghai, China). 3-Aminopropyltrimethoxysilane (APS) was purchased from Alfa Aesar Inc. (Beijing, China). All chemicals were used without further purifications. Doubled distilled water was used in all experiments.

Field emission scanning electron microscopy (FESEM) measurements were performed on a Hitachi S-4800 scanning electron microscopy. Transmission electron microscopy (TEM) measurements were examined using a JEM model 100SX electron microscopes (Japan Electron CO.) operated at an accelerating voltage at 80 kV. UV-Visible absorption spectra were recorded using a spectrophotometer (TU-1901, Beijing Puxi Inc., China). The phase structure and phase purity of the as-synthesized products were examined by X-ray diffraction (XRD) using an X-ray diffractometer (MAC Science Co. Ltd., MXP 18 AHF) with a monochromatized Cu Kα radiation ($\lambda = 1.54056$ Å).

Synthesis of 50 nm gold nanoparticles

According to literature,[30] gold nanoparticles with 50 nm diameters were prepared. Briefly, a seed solution of 13 nm-diameter gold nanoparticles was prepared by adding 5 mL of 38.8 mM sodium citrate solution into 50 mL of 1 mM boiling HAuCl$_4$ solution with vigorous stirring for 15 min. After cooling to room temperature, the as-prepared 1.12 mL seed solution and 0.56 mL of 38.8 mM sodium citrate solution were injected into 125 mL of 0.296 mM boiling aqueous solution of HAuCl$_4$ under the rapid magnetic stirring. The mixture was then boiled for 30 min. Next, additional 5 mL of 38.8 mM sodium citrate solution, as the extra stabilizer, was added into the boiling solution, which was then heated for another one hour.

Synthesis of silica-coated Au nanoparticles

The as-prepared 1.5 mL Au nanoparticles colloids with 50 nm diameters were mixed with 5 mL isopropanol in a 50 mL polypropylene conical tube. Under vigorous shaking, 0.125 mL ammonia (30 wt.%) was added to the mixture, followed by the addition of TEOS in 0.6 mL of 10 mM isopropanol four times within 6 h (at a time interval of 2 h). After reacting for 18 h, another 0.6 mL TEOS in isopropanol was added into the reaction mixture four times within 6 h followed by another 18 h reaction period. The reaction mixture was centrifuged at 4000 rpm for 5 min; the precipitate was washed with isopropanol for three times. Then, Au@SiO$_2$ nanoparticles were obtained and dispersed into ethanol for application for the next step.

Synthesis of titania coating of Au/SiO$_2$ and Au/SiO$_2$@TiO$_2$ spheres

In a typical experiment, Au/SiO$_2$ spheres were sonicated in 20 mL of ethanol. The dispersed suspension solution was mixed with 30 mL of ethanol which contain 0.32 M H$_2$O and 0.0091 M TBOT. The final mixture was refluxed and magnetically stirred for 1.5 h.

Monodispersed Au/SiO$_2$ spheres were synthesized as the literature described.[26] In brief, as-prepared Au/SiO$_2$ spheres dispersed by supersonic in ethanol was mixed with a certain amount of TBOT and water. More ethanol was added to make a total volume of 50 mL. The concentration of TBOT was kept at 0.0091 M and that of water at 0.32 M. The final mixture was refluxed for 1.5 h with continuous stirring. The products were separated centrifugally and washed three times. The resulting TiO$_2$-coating spheres were redispersed in ethanol before use. The above procedure was repeated several times in order to increase the coating thickness. The Au/SiO$_2$@TiO$_2$ was calcined in air at 500 °C (2 °C min^{-1}) for 2 h to remove all organic compounds and crystallize the amorphous TiO$_2$.

Photocatalytic measurements

According to the relevant literatures,[31-33] the details of photocatalysis tests of methyl orange were as follows: methyl orange was used as a simulated contaminant to evaluate the photocatalytic activity of the Au/SiO$_2$@TiO$_2$ core shell nanocomposites. The schematic illustration was shown in Scheme 1. In the test, 50 mL of 1×10^{-5} mol L^{-1} methyl orange dyes solution and 50 mg Au/SiO$_2$@TiO$_2$ core shell nanocomposites were placed in a 70 mL weighing bottle. The suspensions were ultrasonically treated for 30 min and magnetically stirred in the dark for 45 min to
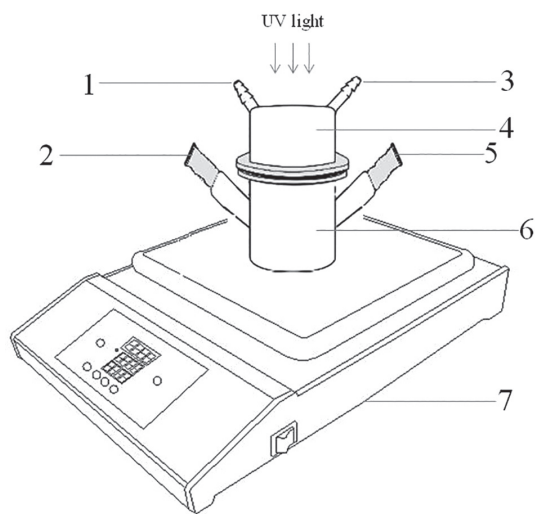
ensure an adsorption/desorption equilibrium. The reaction suspensions containing methyl orange and nano-sized $Au/SiO_2@TiO_2$ photocatalysts were left in homemade photo reactor. A series of photo degradation reactions under the same conditions were performed while a 125 W high-pressure Hg lamp ($\lambda_{max} = 365$ nm) was used. The light was cooled with flowing water in a quartz cylindrical jacket. The distance between the light and the reaction tube was fixed at 15 cm. The analytical samples were taken at regular intervals, centrifuged and filtered. Meanwhile, doubled distilled water with the same volume was added immediately after 1 mL sample was taken. The concentrations of methyl orange were monitored by checking the absorbance at 464 nm during the photo degradation process by using a TU-1901 model UV-Vis spectrophotometer (TU-1901, Beijing Puxi Inc., China). The photocatalytic efficiency (η) was calculated from the expression $\eta = (1 - A / A_0)$, where A_0 is the absorbance of methyl orange before illumination and A is the absorbance of methyl orange after a certain irradiation time.

Results and Discussion

For reviewing the building process of $Au/SiO_2@TiO_2$, the samples of different stage were real time detected by UV-Vis spectra. Figure 1a shows the UV-Vis spectra of Au colloid solution, the characteristic absorption peak appears at 520 nm, that corresponds to plasma resonance absorption of Au nanoparticles, which is in accordance with literature.[34,35] The absorption spectrum of the $Au@SiO_2$ and $Au/SiO_2@TiO_2$ colloids in ethanol exhibits a plasma absorption band at 535 and 550 nm, respectively. The optical properties of Au nanoparticles can be controlled by variation of the composition of the shell layer which is consistent with the theoretical prediction that surface plasmon resonance energies decrease as the refractive index of the surrounding medium increases.[36,37] The presence of the SiO_2 (n = 1.4) and TiO_2 (n = 2.5) shell causes the plasmon absorption peak to shift to the red region. This is reasonable, because the surface plasmon resonance (SPR) absorption of Au nanoparticles is sensitive to the surrounding environment.[38] The small difference between Figure 1a and Figure 1c is attributed to the interfacial changes associated with UV irradiation.[39]

Au and $Au@SiO_2/TiO_2$ nanoparticles were obtained after separating via centrifugation and cleaning by absolute ethanol. Figure 2 shows TEM images of gold nanoparticles (a) and $Au@SiO_2/TiO_2$ core-shell nanoparticles (b, c). As shown in the TEM images of Figure 2 the gold alone and composite nanoparticles are in well-dispersed spherical shape and the mean diameters of particles are 50 and 170 nm, respectively. That is to say,

Scheme 1. Schematic of experimental apparatus for photocatalysis tests: (1) water in; (2) doubled distilled in; (3) water out; (4) water; (5) sample out; (6) samples and photocatalysts; (7) mechanical stirrer.
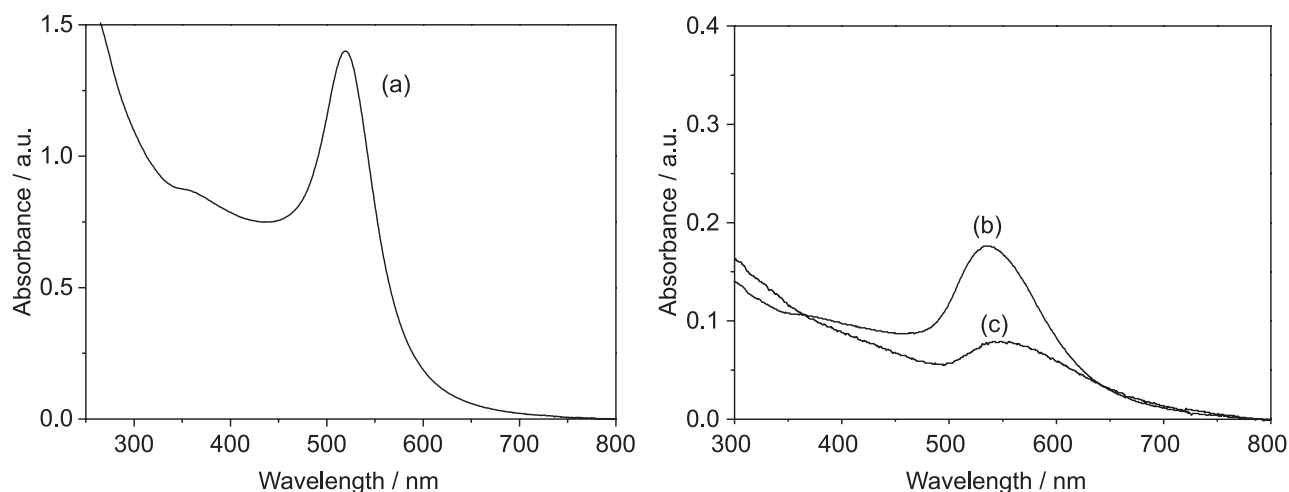
Figure 1. UV-Vis spectra: (a) Au nanoparticles; (b) Au/SiO_2; (c) $Au/SiO_2@TiO_2$.

the thickness of shell is circa 60 nm. The darker color is the electron dense Au, the brighter is SiO_2 and TiO_2. The obvious boundaries cannot be found between SiO_2 and TiO_2 layer, because the electron density of SiO_2 and TiO_2 is similar.

According to relevant literature[40] in the process of formation of Au/SiO₂@TiO₂ coating particles, SiO_2 particles play an important role. The seed SiO_2 particles provide a new scenario for the precipitation and formation of TiO_2. Accompany the precipitation of TiO_2 as a new phase, the processes are as followed. At first, the reactants of TiO_2 will be absorbed by SiO_2 particles, and the new phase can directly precipitate on the surface of seed particles. Then, the new phase will form nanosized particles, precipitating separately in solutions, which then interact with and adhere to the surface of other particles. When the concentration of nanoparticles in the system reaches a certain amount, new phase of Au/SiO₂@TiO₂ will precipitate. The result is that the seed particles and the newly precipitated phase coexist as separate phases.

Figure 3 shows the typical FESEM images of the as-synthesized core-shell Au@SiO₂ and Au@SiO₂/TiO₂ nanocomposites. The inserting pictures in the top left corner are at higher magnification. Clearly, perfect spheres with a mean size of 150 nm are evenly distributed in Figure 3a. With the formation of TiO_2 layer, the size of composite microspheres had increased to 170 nm, and the relatively smooth surface became rough. It can be deduced that the thickness of TiO_2 layer is about 10 nm. The monodispersity of samples have improved.

In order to investigate the distribution of surface elements of Au@SiO₂/TiO₂ nanoparticles, the products were analyzed by X-ray photoelectron spectroscopy (XPS) scanning. Characteristic peaks of Au^0 at 87.1 eV (Au $4f_{5/2}$) and 83.4 eV (Au $4f_{7/2}$) are observed (shown in Figure 4a). Figure 4b displays electron bonding energy peak of Ti 2p
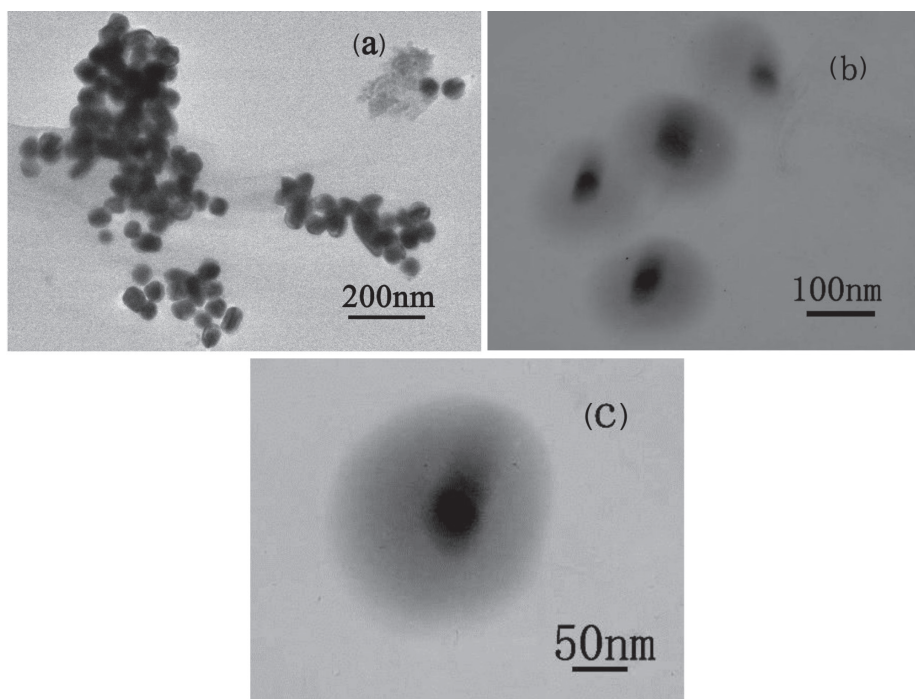

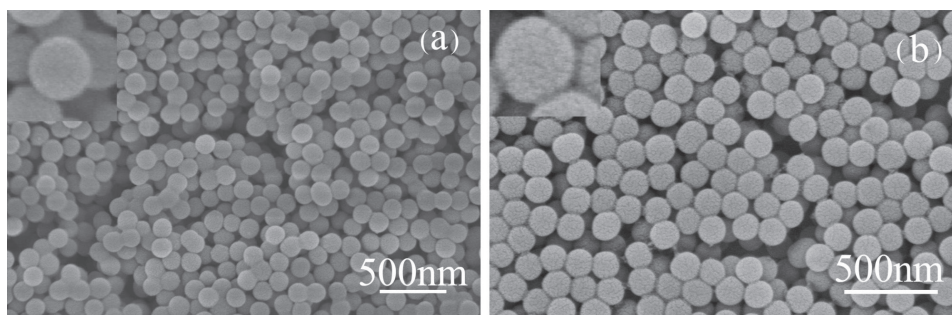**Figure 2.** TEM images of (a) Au; (b, c) Au@SiO₂/TiO₂ nanoparticles.

Figure 3. FESEM images of (a) Au@SiO₂ and (b) Au@SiO₂/TiO₂; the insets show the high-resolution image of single particle in the top left corner.

orbital, and it can be seen that the appearance of two peaks located at around 457.1 and 462.8 eV, which can be assigned to Ti 2p$_{3/2}$ and Ti 2p$_{1/2}$ bonding energy, respectively. It indicates that Ti is +4 valence states, which is consistent with literature values.[41] Figure 4c shows the Si XPS spectra which peaks were fitted on the map. There are two peaks at 102.1 and 104.6 eV, which is corresponding to Si 2p$_{3/2}$ and Si 2p$_{1/2}$ photoelectron peaks. Compared with Si 2p$_{3/2}$ and Si 2p$_{1/2}$ photoelectron peaks in the standard SiO$_2$ (103.6, 104.0 eV), the optical electronic peak of Si 2p$_{3/2}$ falls 1.5 eV. There are two peaks at 528.6 and 532.5 eV through Gaussian peak fitting (Figure 4d), which are directed to the photoelectron peaks of O1s orbit. Peak at 528.6 eV corresponds to the lattice oxygen, which reduces 1.1 eV compared with the SiO$_2$ or TiO$_2$ standard lattice O bonding (529.7 eV). It may be caused by the formation of Ti–O–Si bonds. The ca. 532.5 eV peak is attributed to the presence of hydroxyl on the product surface. Therefore, the XPS results demonstrate that the TiO$_2$ and SiO$_2$ exist on the product surface.

The XRD patterns of the as-synthesized Au/SiO$_2$@TiO$_2$ nanoparticles before and after calcination were shown in Figure 5. It could be seen that the diffraction peaks at 2θ = 38.3, 44.6, 64.7, 77.8 and 81.84°, assigned to (111), (200), (220), (311) and (222) planes of Au nanoparticles (JCPDS No. 04-0784) reveal that the synthesized gold nanoparticles are composed of pure crystalline gold. The average crystallite size of Au can be calculated by applying the Debye-Scherrer formula (equation 1).

$$D = K\lambda / \beta\cos\theta \tag{1}$$

where D is the average crystallite size, K is a constant which is taken as 0.89 here, λ is the wavelength of the X-ray radiation (Cu Kα, λ = 1.54056 nm), β is the corrected band broadening (full width at half-maximum (FWHM)) after subtraction of equipment broadening, and θ is the diffraction angle. The average crystallite sizes of samples Au is about 47 nm.

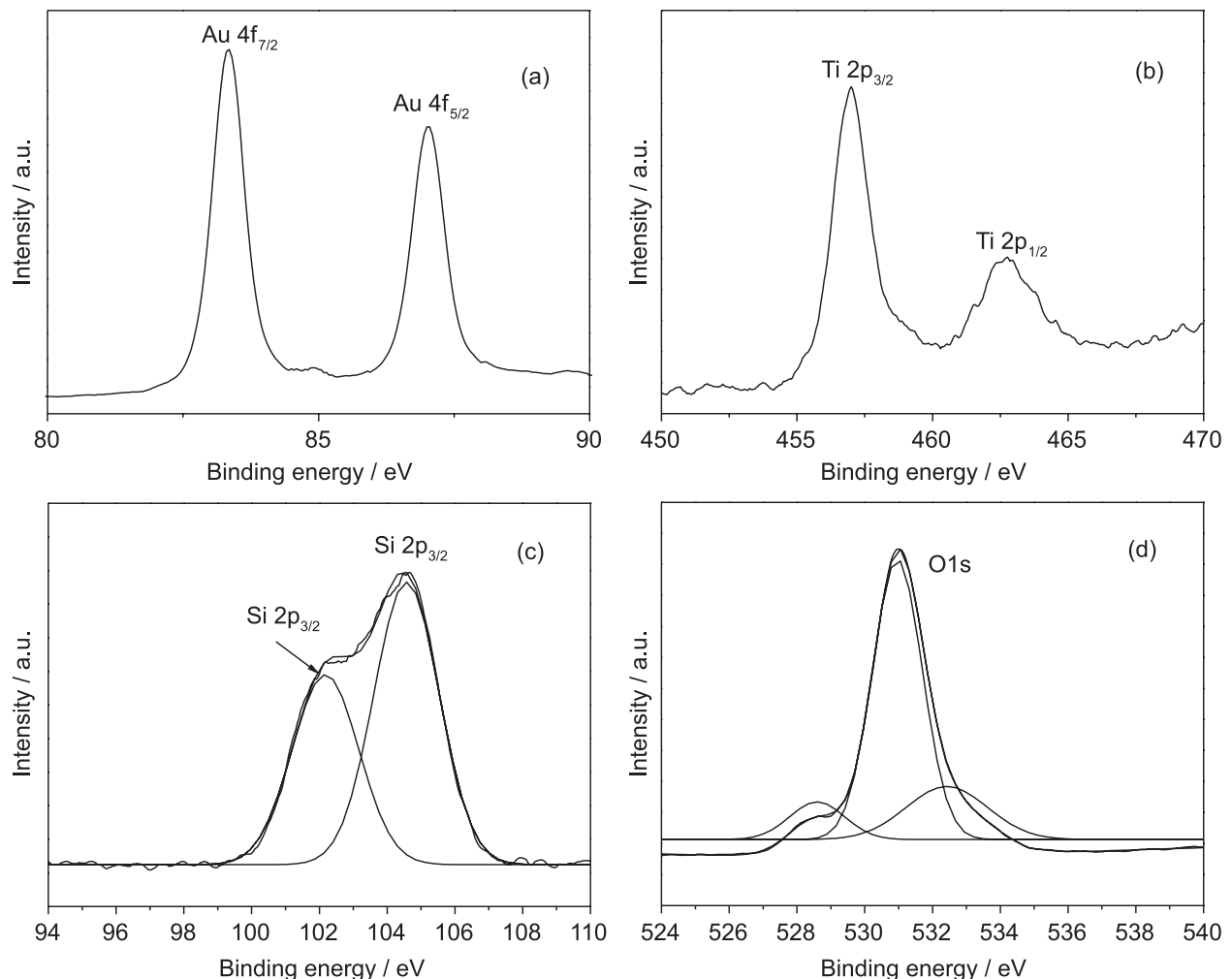Core-shell Au-TiO$_2$ composite nanoparticles were found

Figure 4. XPS spectra of Au/SiO$_2$@TiO$_2$: (a) XPS survey scan of the Au@SiO$_2$/TiO$_2$; high-resolution XPS spectra of particles for (b) Ti; (c) Si; (d) O.
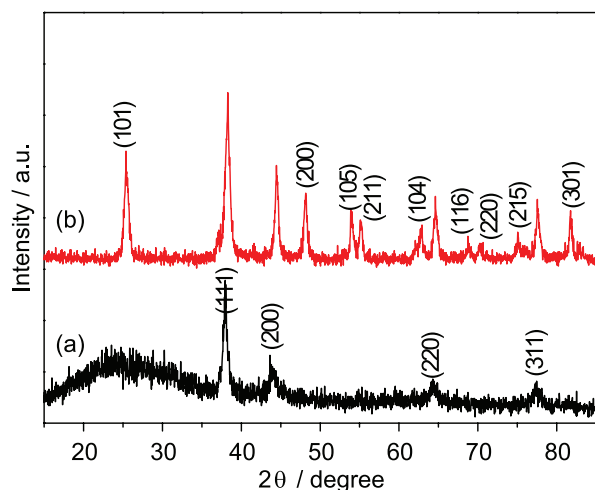
Figure 5. X-ray diffraction patterns of Au/SiO₂@TiO₂: (a) uncalcined; (b) calcined.

to keep the diffraction peaks characteristic of Au crystal. However, there were no characteristic diffraction peaks of SiO₂ and TiO₂ before calcination Au-titania composite nanoparticles, which suggested that the SiO₂ and TiO₂ shell was amorphous. After calcination, the pattern (Figure 5b) proves the structure of anatase of the TiO₂ shell with lattice constant a = 3.782 Å (JCPDS No. 84-1286). As shown in Figure 5b, the typical diffraction peaks at 25.4, 48.2, 54.1, 55.2, 62.8, 68.8, 70.5, 75.1 and 76.1° can be ascribed to the (101), (200), (105), (211), (204), (116), (220), (215), and (301) faces of anatase TiO₂.

Although methyl orange is a photo stable substance, it can be photo degraded in the presence of ultraviolet light with appropriate catalyst. The methyl orange concentration was measured from the absorbance at the wavelength of 464 nm by using a calibration curve (as shown in Figure 6a). The degradation rate of methyl orange was calculated from the absorbance. As can be seen, in the 20 min photocatalytic

effect is very obvious, the initial degradation rate of 5 min reached 30%; after 20 min, the degradation rate reached 80%; after 2 h, methyl orange was almost completely degraded (as shown in Figure 6b).

The samples showed good photocatalytic performance which maybe depend on effective separate of electronic-hole pairs. Figure 7a shows the covalent bond and conduction band energy of TiO₂, adsorbed oxygen on the surface of TiO₂, gold nanoparticles, which can determine the direction of electron flow.[42-44] When the gold is wrapped into the titanium dioxide shell, the electron has difficulty to move from gold to adsorbed oxygen on the titanium dioxide, because energy level of adsorbed oxygen is higher than the level of gold. Normally, the Fermi level of the metal particles increases with the decrease of the particle size, this is the result of quantum size effect. Thus, when the gold nanoparticles reach the appropriate size, their energy levels may be in between the conduction band of TiO₂ and adsorbed oxygen. These photoelectrons absorbed via TiO₂ are captured by the gold nanoparticles, and transfer to the adsorbed oxygen, causing the separation of electrons and holes. The gold nuclei inside is filled with electrons, and the TiO₂ shell gathers a lot of holes due to the loss of electrons. When the size of Au NPs is big enough, the gold nanoparticles' Fermi level is lower than the Fermi level of adsorbed oxygen; the photoelectron cannot be transferred to the adsorbed oxygen. If the size of gold nanoparticles is too small, photoelectron may not transfer from the conduction band of TiO₂ to the Au nanoparticles, because of the gold nanoparticles' Fermi level exceeds the Fermi level of adsorbed oxygen. In as-prepared of core-shell structure, the photoelectrons are captured and stored in the gold core (as shown in Figure 7b) and will not immediately transfer to the adsorbed oxygen on the TiO₂ shell. Electrons are bound within the nucleus for a
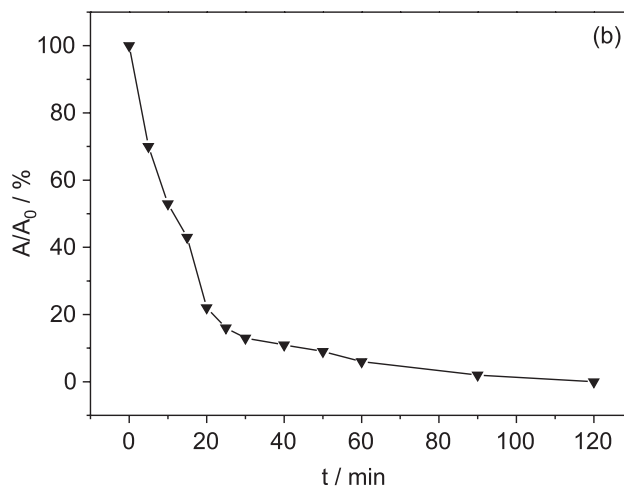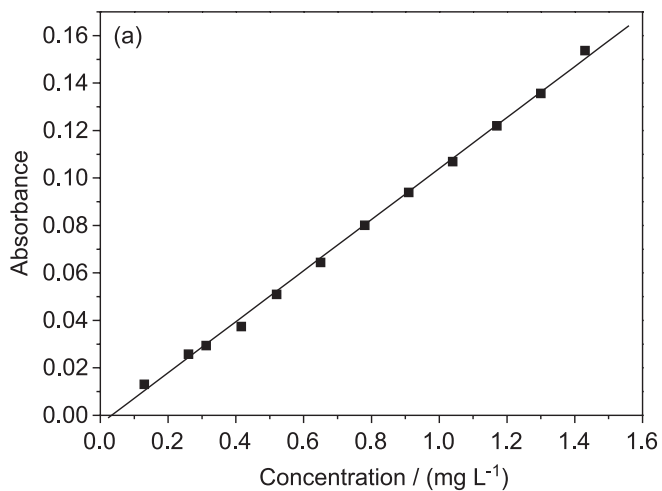

Figure 6. (a) Calibration curve of MO solution; (b) photocatalytic degradation efficiency of MO over photocatalyst.
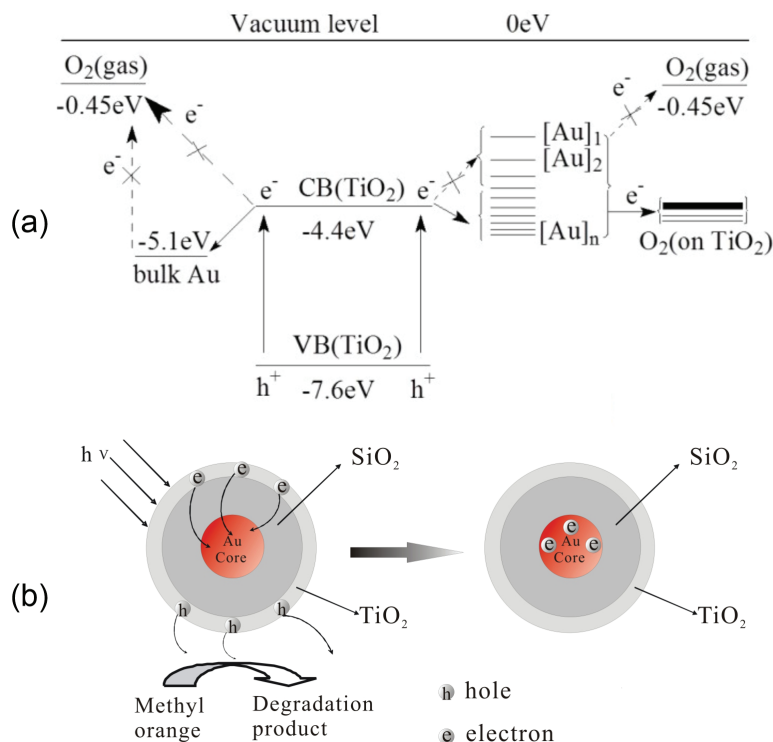
Figure 7. The mechanism of photocatalysis: (a) the schematic diagram[27] showing the electronic energy levels of Au nanoparticle, valence band (VB), and conduction band (CB) of TiO_2 and adsorbed O_2; (b) photoinduced charge injection and charge separation.

relatively long time, extending the recombination time of hole with electron. Thus, the number of holes is increased, and the photocatalytic performance is enhanced. After $Au/SiO_2@TiO_2$ acting as catalyst, the degradation efficiency of MO is high, because the Au nanoparticles can serve as electron traps. Under UV light irradiation, photogenerated electrons and holes are efficiently separated and increased the photocatalytic reaction activity. The coating of SiO_2 insulate the Au particles, thus blocking out the photogenerated electrons from TiO_2.[45]

Conclusions

In summary, $Au/SiO_2@TiO_2$ core-shell nanostructures are synthesized by the sol-gel method and ethanol reflux synthesis steps with calcination. Photocatalytic degradation of methyl orange in the liquid phase has been carried out to evaluate photocatalytic performance under UV light irradiation. $Au/SiO_2@TiO_2$ core-shell nano-composite possesses ideal photocatalytic activity since it has the suitable decoration amount of Au nanoparticles for harvesting the UV light energy by their plasmonic effects and for prohibiting the recombination of free excitons by serving as an electron reservoir. The presence of the kernel of gold nanoparticles leads to separation of electron hole pair, electron is transferred to the gold nanoparticles in the nucleus, and thus is stored; the outer TiO_2 will be enriched

holes, thereby increasing the photocatalytic degradation effect. Due to the effective separation of charge, the special structure of the material is also expected to have a good application prospects in solar cells.

Acknowledgments

References

1. Kenens, B.; Chamtouri, M.; Aubert, R.; Miyakawa, K.; Hayasaka, Y.; Naiki, H.; Watanabe, H.; Inose, T.; Fujita, Y.; Lu, G.; Masuhara, A.; Uji-i, H.; *RSC Adv.* **2016**, *6*, 97464.

2. Lacombe, S.; Pigot, T.; *Catal. Sci. Technol.* **2016**, *6*, 1571.

3. Bian, Z.; Tachikawa, T.; Zhang, P.; Fujitsuka, M.; Majima, T.; *J. Am. Chem. Soc.* **2014**, *136*, 458.

4. Lu, J.; Lan, L.; Liu, X. T.; Wang, N.; Fan, X.; *Front. Chem. Sci. Eng.* **2019**, DOI: 10.1007/s11705-019-1815-2.

5. El-Ashtoukhy, E. Z.; Amin, N. K.; El-Latif, M. A.; Bassyouni, D. G.; Hamad, H. A.; *J. Cleaner Prod.* **2017**, *167*, 432.

6. Abbasi, A.; Ghanbari, D.; Salavatiniasari, M.; Hamadanian, M.; *J. Mater. Sci.: Mater. Electron.* **2016**, *27*, 4800.

7. Okuno, T.; Kawamura, G.; Muto, H.; Matsuda, A.; *J. Solid State Chem.* **2016**, *235*, 132.

8. Safajou, H.; Khojasteh, H.; Salavati-Niasari, M.; Mortazavi-Derazkola, S.; *J. Colloid Interface Sci.* **2017**, *498*, 423.

9. Yang, Y.; Ma, Z.; Xu, L.; Wang, H.; Fu, N.; *Appl. Surf. Sci.* **2016**, *369*, 576.

10. Jiao, J.; Wei, Y.; Zhao, Z.; Zhong, W.; Liu, J.; Li, J.; Duan, A.; Jiang, G.; *Catal. Today* **2015**, *258*, 319.

11. Li, J.; Wu, N.; *Catal. Sci. Technol.* **2015**, *5*, 1360.

12. El Essawy, N. A.; Ali, S. M.; Farag, H. A.; Konsowa, A. H.; Elnouby, M.; Hamad, H. A.; *Ecotoxicol. Environ. Saf.* **2017**, *145*, 57.

13. Majeed, I.; Nadeem, M.; Al-Oufi, M.; Waterhouse, G.; Badshah, G.; Metson, J.; Idriss, H.; *Appl. Catal., B* **2016**, *182*, 266.

14. Khojasteh, H.; Salavati-Niasari, M.; Abbasi, A.; Azizi, F.; Enhessari, M.; *J. Mater. Sci.: Mater. Electron.* **2016**, *27*, 1261.

15. Yoo, S. M.; Rawal, S. B.; Lee, J. E.; Kim, J.; Ryu, H. Y.; Park, D. W.; Lee, W. I.; *Appl. Catal., A* **2015**, *499*, 47.

16. Frey, W.; Woods, C.; Chilkoti, A.; *Adv. Mater.* **2000**, *12*, 1515.

17. Su, R.; Tiruvalam, R.; He, Q.; Dimitratos, N.; Kesavan, L.; Hammond, C.; Lopez-Sanchez, J.; Bechstein, R.; Kiely, C.; Hutchings, G.; Besenbacher, F.; *ACS Nano* **2012**, *6*, 6284.

18. Sabet, M.; Salavati-Niasari, M.; Amiri, O.; *Electrochim. Acta* **2014**, *117*, 504.

19. Ye, X.; Cai, S.; Zheng, C.; Xiao, X.; Hua, N.; Huang, Y.; *Appl. Surf. Sci.* **2015**, *345*, 279.

20. Youn, N.; Heo, J.; Joo, O.; Lee, H.; Kim, J.; Min, B.; *J. Hazard. Mater.* **2010**, *177*, 216.

21. Hamad, H.; Bassyouni, D.; El-Ashtoukhy, E. S.; Amin, N.; El-Latif, M. A.; *Ecotoxicol. Environ. Saf.* **2018**, *148*, 501.

22. Liu, Z.; Hou, W.; Pavaskar, P.; Aykol, M.; Cronin, S.; *Nano Lett.* **2011**, *11*, 1111.

23. Tanaka, A.; Hashimoto, K.; Kominami, H.; *J. Am. Chem. Soc.* **2012**, *134*, 14526.

24. Long, R.; Prezhdo, O.; *J. Am. Chem. Soc.* **2014**, *136*, 4343.

25. Jiang, T.; Jia, C.; Zhang, L.; He, S.; Sang, Y.; Li, H.; Li, Y.; Xu, X.; Liu, H.; *Nanoscale* **2015**, *7*, 209.

26. Zhan, X.; Bao, Y.; Wang, F.; Wang, Q.; Cheng, Z.; Wang, Z.; Xu, K.; Fang, Z.; He, J.; *Appl. Phys. Lett.* **2015**, *106*, 123904.

27. Gholami, T.; Bazarganipour, M.; Salavati-Niasari, M.; Bagheri, S.; *J. Mater. Sci.: Mater. Electron.* **2015**, *26*, 6170.

28. Mortazavi-Derazkola, S.; Salavati-Niasari, M.; Amiri, O.; Abbasi, A.; *J. Energy Chem.* **2017**, *1*, 27.

29. Shalaby, T.; Hamad, H.; Ibrahim, E.; Mahmoud, O.; Al-Oufy, A.; *Ecotoxicol. Environ. Saf.* **2018**, *162*, 354.

30. Qi, Y.; Chen, M.; Liang, S.; Yang, W.; Zhao, J.; *Appl. Surf. Sci.* **2008**, *254*, 1684.

31. Tian, B.; Tong, T.; Chen, F.; Zhang, J.; *Acta. Phys.-Chim. Sin.* **2007**, *23*, 978.

32. Fathy, M.; Hamad, H.; Kashyout, A. E. H.; *RSC Adv.* **2016**, *6*, 7310.

33. Hamad, H.; Bailón-García, E.; Morales-Torres, S.; Carrasco-Marín, F.; Pérez-Cadenas, A. F.; Maldonado-Hódar, F. J.; *J. Environ. Chem. Eng.* **2018**, *6*, 5032.

34. Brust, M.; Walker, M.; Bethell, D.; Schiffrin, J. D.; Whyman, R.; *Chem. Commun.* **1994**, *7*, 801.

35. Sandhyarani, N.; Resmi, M.; Unnikrishnan, R.; Vidyasagar, K.; Ma, S.; Antony, M.; Panneer, S.; Visalakshi, V.; Chandrakumar, N.; Pandian, K.; Tao, Y.; Pradeep, T.; *Chem. Mater.* **2000**, *12*, 104.

36. Templeton, A.; Pietron, J.; Murray, R.; Mulvaney, P.; *J. Phys. Chem. B* **2000**, *104*, 564.

37. Kang, Y.; Taton, T.; *Angew. Chem., Int. Ed.* **2005**, *44*, 409.

38. Zhang, N.; Liu, S.; Fu, X.; Xu, Y.; *J. Phys. Chem. C* **2011**, *115*, 9136.

39. Hirakawa, T.; Kamat, P.; *Langmuir* **2004**, *20*, 5645.

40. Hamad, H.; El-Latif, M. A.; Kashyout, A. E. H.; Sadik, W.; Feteha, M.; *New J. Chem.* **2015**, *39*, 3116.

41. Guin, D.; Manorama, S.; Latha, J.; Singh, S.; *J. Phys. Chem. C* **2007**, *111*, 13393.

42. Hamad, H.; Bailon-Garcia, E.; Maldonado-Hódar, F. J.; Perez-Cadenas, A. F.; Carrasco-Marin, F.; Morales-Torres, S.; *Appl. Catal., B* **2019**, *241*, 385.

43. Altunata, S.; Cunningham, K.; Canagaratna, M.; Thom, R.; Field, R.; *J. Phys. Chem. A* **2002**, *106*, 1122.

44. Hamad, H.; El-latif, M. A.; Kashyout, A. E.-H.; Sadik, W.; Feteha, M.; *Process Saf. Environ. Prot.* **2015**, *98*, 390.

45. Chen, J. J.; Wu, J. C. S.; Wu, P. C.; Tsai, D. P.; *J. Phys. Chem. C* **2012**, *116*, 26535.